

Diffusion measurement from observed transverse beam echoes

Tanaji Sen

*Accelerator Physics Center, FNAL, Batavia, IL 60510**

Wolfram Fischer

BNL, Upton, NY 11973

Abstract

We study the measurement of transverse diffusion through beam echoes. We revisit earlier observations of echoes in RHIC and apply an updated theoretical model to these measurements. We consider three possible models for the diffusion coefficient and show that only one is consistent with measured echo amplitudes and pulse widths. This model allows us to parameterize the diffusion coefficients as functions of bunch charge. We demonstrate that echoes can be used to measure diffusion much quicker than present methods and could be useful to a variety of hadron synchrotrons.

* tsen@fnal.gov

I. INTRODUCTION

Beam diffusion can lead to emittance growth, halo formation and particle loss. A standard method currently used to measure transverse diffusion requires scraping the beam with collimator jaws moved close to the beam, then retracting the jaws and waiting for the beam to diffuse to the outer position of the jaws [1–5]. This procedure is time consuming and the method is only applicable to storage rings where the beam circulates for times long enough to enable the measurement. Beam echoes were introduced into accelerator physics more than two decades ago [6, 7] and then shown to be useful as a novel method to measure transverse diffusion [8]. A single echo observation can be done typically within a thousand turns with nonlinear tune spreads in the range 0.001 - 0.01. Hence diffusion measurements with echoes would be considerably faster than the standard method and could also enable diffusion to be measured in synchrotrons where beams circulate for relatively short times.

Shortly after the introduction of the beam echo concept, longitudinal unbunched beam echoes were observed at the Fermilab Antiproton Accumulator [9] and then at the CERN SPS [10]. The original motivation however had been to measure transverse diffusion from transverse echoes. In the year 2000, transverse bunched beam echoes were observed in the SPS with two consecutive dipole kicks [11] but no diffusion coefficients were extracted. Later in 2004-2005 an extensive set of dedicated experiments was carried out at RHIC with dipole and quadrupole kicks [12] and these will be the focus in this paper. The existing model as applied to the data did not yield consistent values for the diffusion coefficients [13].

The next generation of intensity frontier hadron synchrotrons will require tight control of particle amplitude growth. At Fermilab the Integrable Optics Test Accelerator (IOTA) [14] ring is under construction where the novel concept of nonlinearly integrable lattices will be tested and could serve as a model for future synchrotrons. This ring offers the opportunity of testing a fast diffusion measurement technique which could help determine the degree of integrability (or stable motion) among different lattice models. With this motivation, we revisit the earlier RHIC measurements with an updated theoretical model to enable extraction of self-consistent diffusion coefficients. In Section II we describe the updated model, in Section III we apply this model to the RHIC data, in Section IV

we consider beam related time scales and we summarize in Section V with lessons to be applied to future echo measurements.

II. ECHO PULSE WITH DIFFUSION

The basic beam echo generating mechanism is well known. If at some initial time the beam is kicked away from the central orbit, the beam centroid will decohere due to a nonlinear spread of frequencies. If subsequently a quadrupole kick is applied after the centroid response has decayed away, a diminished coherent response will reappear after a time interval equal to the delay between the dipole and quadrupole kicks. Figure 5 in Section III C shows an example of this echo formation during the measurements at RHIC.

Here we discuss the model to calculate the echo amplitude with diffusion using the same method and notation as in [15]. The phase space coordinates used x, p and action angle coordinates J, ϕ are related as

$$x = \sqrt{2\beta J} \cos \phi, \quad p = \alpha x + \beta x' = -\sqrt{2\beta J} \sin \phi \quad (1)$$

$$J = \frac{1}{2\beta}(x^2 + p^2), \quad \tan \phi = -\frac{p}{x} \quad (2)$$

The initial distribution is taken to be exponential in the action

$$\psi_0(J) = \frac{1}{2\pi J_0} \exp\left[-\frac{J}{J_0}\right] \quad (3)$$

where $J_0 = \varepsilon_0$, the initial rms emittance.

We first consider the dipole moment after a dipole kick and the general case where the dipole kicker is at a non-zero phase advance from the BPM location where the centroid is measured. Following the procedure in [15], the dipole moment after the dipole kick by an angle θ is

$$\langle x \rangle^{amp}(t) = \frac{\theta \sqrt{\beta_K \beta}}{(1 + \Theta^2)} \exp\left[-\frac{\beta_K \theta^2}{2J_0} \frac{\Theta^2}{1 + \Theta^2}\right] \quad (4)$$

where β_K, β are the beta functions at the kicker and BPM respectively, $\Theta = \omega' J_0 t$ with $\omega' \equiv d\omega/dJ$ the constant slope of the betatron angular frequency with action. This moment is independent of the phase advance from the kicker to the BPM. It differs from the expression

in [15] only by the replacement of β by the geometric mean $\beta_G = \sqrt{\beta_K \beta}$ and β in the exponent replaced by β_K . Following the dipole kick, the beam decoheres with the centroid amplitude decaying over a characteristic time $\tau_D = 1/(\omega' J_0)$, the decoherence time. At time $\tau \gg \tau_D$ after the dipole kick, a single turn quadrupole kick is applied to generate the echoes, the first of which occurs around time 2τ . The echo amplitude and pulse shape is affected by the diffusive beam motion. We consider the density distribution to evolve according to the conventional form of the diffusion equation

$$\frac{\partial}{\partial t} \psi = \frac{\partial}{\partial J} [D(J) \frac{\partial}{\partial J}] \psi \quad (5)$$

Here the diffusion coefficient $D(J)$ has the usual dimension of [action²/time] and it differs from the definition of $D(J)$ used in [8, 15]. The treatment in [15] had developed the theory of the echo response to first order in the quadrupole kick strength. Since the experiments reported in [12] had observed a linear increase of the echo amplitude with quadrupole strength, this theory should suffice to discuss these experiments. We note that the theory developed earlier in [7] was nonlinear in this strength parameter. Using the method of [15], we find that the echo amplitude near time $t > 2\tau$ is

$$\langle x \rangle(t) = -\pi \beta_K \theta q \tau \int dJ \omega' J^2 \psi'_0 \exp[-\frac{1}{3} D(J) (\omega')^2 t_1^3] \sin(\omega(t - 2\tau)) \quad (6)$$

where q is the dimensionless quadrupole kick strength defined as $q = \beta_Q/f$, the ratio of the beta function at the quadrupole to its focal length and we defined $t_1^3 = (t - \tau)^3 + \tau^3$. We consider the action dependent transverse angular frequency to be of the form $\omega(J) = \omega_\beta + \omega' J$ where ω_β is the angular betatron frequency and we consider the diffusion coefficient to be of the form

$$D(J) = \sum_{n=0} D_n \left(\frac{J}{J_0}\right)^n \quad (7)$$

where all coefficients D_n have the same dimensions. The average dipole moment is given by

$$\langle x \rangle(t) = \frac{1}{2} \beta_K \theta q \mu \tau \omega_{rev} \exp[-\frac{1}{3} D_0 (\omega')^2 t_1^3] \text{Im}[e^{i\Phi_0}] \int_0^\infty z^2 \exp[-z - \frac{1}{3} (\omega')^2 t_1^3 \sum_n D_n z^n] e^{i\Phi_1 J_0 z} dz \quad (8)$$

where ω_{rev} is the angular revolution frequency, $\Phi_0 = \omega_\beta(t - 2\tau)$ and $\Phi_1 = \omega'(t - 2\tau)$. Using $\omega' = (\omega_{rev}/\varepsilon)\mu$ where $\mu = v(\varepsilon) - v_\beta$ is the tune shift (from the bare tune v_β) at an

action equal to the emittance, it is convenient to define scaled diffusion coefficients d_n as

$$d_n = \frac{2}{3} D_n \left(\frac{\omega_{rev}}{\epsilon} \right)^2 \quad (9)$$

These coefficients d_n have the dimension of time^{-3} . In the following we will consider specific cases of the above general form of $D(J)$.

Different physical processes contribute to the diffusion coefficients D_n . It is likely that space charge effects, beam-beam interactions (not present in the RHIC measurements discussed below) and intra-beam scattering all contribute to D_0 and higher order coefficients. Early studies at the Tevatron at injection energy [16] with additional sextupoles as the driving nonlinearity had measured a constant D_0 term which varied with the proximity to a fifth order resonance. Measurements at the LHC at top energy during collisions showed that diffusion at the smallest amplitude measurable was finite [4], implying a non-zero D_0 . A numerical simulation [17] showed that modulation diffusion leads to a constant diffusion term. Beam-gas scattering and noise in dipoles lead to a D_1 term while noise in quadrupoles leads to a D_2 term. There are likely other sources for these coefficients. Given that the beam is subject to multiple effects, the complete action dependence of the diffusion may be complex. Here we focus on the three simplest models with two diffusion coefficients that can be compared to measurements.

In the first case, we assume that the diffusion is of the form

$$D(J) = D_0 + D_1 \left(\frac{J}{J_0} \right) \quad (10)$$

in this case, the dipole moment is given by

$$\langle x \rangle(t) = \beta_K \theta q \omega' \tau J_0 \exp\left[-\frac{1}{2} d_0 \mu^2 t_1^3\right] \frac{[(3\alpha^2 - \xi^2)\xi \cos \Phi_0 + (\alpha^2 - 3\xi^2)\alpha \sin \Phi_0]}{(\alpha^2 + \xi^2)^3} \quad (11)$$

$$t_1^3 = (t - \tau)^3 + \tau^3, \quad \Phi_0 = \omega_\beta(t - 2\tau), \quad \alpha = 1 + \frac{1}{2} d_1 \mu^2 t_1^3, \quad \xi = \omega_{rev} \mu(t - 2\tau)$$

The second case is the quadratic dependence model where

$$D(J) = D_0 + D_2 \left(\frac{J}{J_0} \right)^2 \quad (12)$$

The general time dependent form of the echo at time $t = 2\tau + \Delta t$ where Δt can have either sign is

$$\langle x(t) \rangle^{amp} = \frac{1}{2} \beta_K \theta q \omega_{rev} \mu \tau \exp[-\frac{1}{2} d_0 \mu^2 t_1^3] \text{Im}[e^{i\Phi_0} H_{02}] \quad (13)$$

$$\begin{aligned} H_{02}(\Delta t) &\equiv \int_0^\infty z^2 \exp[-a_0 z - b_2 z^2] dz \\ &= \frac{1}{8} \left(\frac{1}{b_2}\right)^{5/2} \left\{ \sqrt{\pi} [a_0^2 + 2b_2] \exp\left(\frac{a_0^2}{4b_2}\right) \text{Erfc}\left(\frac{a_0}{\sqrt{2b_2}}\right) - a_0 \sqrt{2b_2} \right\} \\ a_0 &= 1 - i\xi = 1 - i\omega_{rev} \mu \Delta t, \quad b_2 = \frac{1}{2} d_2 \mu^2 t_1^3 = \frac{1}{2} d_2 \mu^2 [(\tau + \Delta t)^3 + \tau^3] \end{aligned} \quad (14)$$

Here Erfc is the complementary error function.

The last case we consider is the linear and quadratic dependence

$$D(J) = D_1 \left(\frac{J}{J_0}\right) + D_2 \left(\frac{J}{J_0}\right)^2 \quad (15)$$

In this case, the time dependent form of the echo at time $t = 2\tau + \Delta t$ is

$$\langle x(t) \rangle^{amp} = \frac{1}{2} \beta_K \theta q \omega_{rev} \mu \tau \text{Im}[e^{i\Phi_0} H_{12}(\Delta t)] \quad (16)$$

$$\begin{aligned} H_{12}(\Delta t) &\equiv \int_0^\infty z^2 \exp[-a_1 z - b_2 z^2] dz \\ &= \frac{1}{8} \left(\frac{1}{b_2}\right)^{5/2} \left\{ \sqrt{\pi} [a_1^2 + 2b_2] \exp\left(\frac{a_1^2}{4b_2}\right) \text{Erfc}\left(\frac{a_1}{\sqrt{2b_2}}\right) - a_1 \sqrt{2b_2} \right\} \\ a_1 &= (1 + b_1) - i\xi, \quad b_1 = \frac{1}{2} d_1 \mu^2 t_1^3 = \frac{1}{2} d_1 \mu^2 [(\tau + \Delta t)^3 + \tau^3] \end{aligned} \quad (17)$$

The left plot in Fig. 1 shows the relative echo amplitude as a function of the diffusion coefficient D_n for three values of n . In each case, only the single D_n was non-zero. For the same value of D_n , the amplitude decreases faster as n increases. The right plot in this figure shows the form of the echo pulse with the D_1, D_2 model for a particular choice of D_1, D_2 and other machine parameters are taken from the RHIC values. The red curve shows the upper envelope of the pulse which is used to obtain the full width at half maximum.

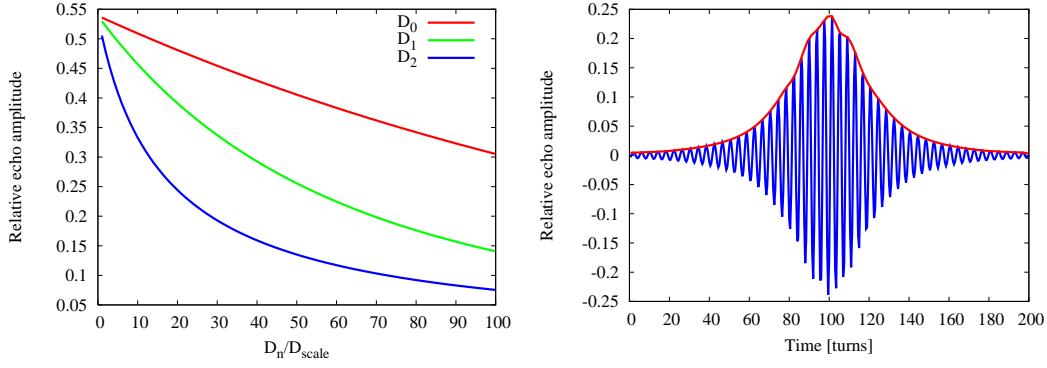


FIG. 1. Left: The echo amplitude as a function of the coefficients D_0, D_1, D_2 scaled by the value $D_{scale} = 2.4 \times 10^{-15} \text{m}^2/\text{s}$. Right: Form of the echo pulse with the D_1, D_2 model shown in blue. The red curve outlines the upper envelope of the echo. Beam parameters in both plots were taken from Table I, except for $\mu = 0.0077$. D_1, D_2 in the right plot were set to the values $D_{1,sc}, D_{2,sc}$ respectively which are defined in Sec. III B.

A. Optimum tune shift and delay time

Analytical results for the optimum values of the tune shift and delay parameters that maximize the echo amplitude can be obtained for model 1 with diffusion coefficients (d_0, d_1) . As a function of the time delay, this amplitude has a maximum at a delay $\tau = \tau_{opt}$, such that the two coefficients can be related as

$$d_1 = \frac{1 - 3d_0\mu_{fix}^2\tau_{opt}^3}{\mu_{fix}^2\tau_{opt}^3(8 + 3d_0\mu_{fix}^2\tau_{opt}^3)} \quad (18)$$

It is understood that μ is held fixed at μ_{fix} while finding the optimum delay τ_{opt} . Defining $c_\tau = \mu_{fix}^2\tau_{opt}^3$ and substituting this into the equation for the relative amplitude, we have for the maximum amplitude obtained at the delay τ_{opt}

$$\frac{\langle x \rangle_{max}(\tau_{opt})}{\beta_K \theta} = \omega_{rev} q \mu \tau_{opt} \left[\frac{8 + 3d_0 c_\tau}{9} \right]^3 \exp[-d_0 c_\tau] \quad (19)$$

This equation can be solved for d_0 and subsequently d_1 can be found. Positivity of d_1 requires that the solution for d_0 obey $3d_0 c_\tau \leq 1$.

Similarly, as a function of the tune shift, the amplitude has a maximum at $\mu = \mu_{opt}$ such that

$$d_1 = \frac{1 - 2d_0\mu_{opt}^2\tau_{fix}^3}{\mu_{opt}^2\tau_{fix}^3(5 + 2d_0\mu_{opt}^2\tau_{fix}^3)} \quad (20)$$

Here τ is held fixed at τ_{fix} while finding the optimum in μ . Defining $c_\mu = \mu_{opt}^2 \tau_{fix}^3$ and again, substituting for d_1 , we can write the maximum relative amplitude at μ_{opt} as

$$\frac{\langle x \rangle_{max}(\mu_{opt})}{\beta_K \theta} = \omega_{rev} q \mu_{opt} \tau_{fix} \left[\frac{5 + 2d_0 c_\mu}{6} \right]^3 \exp[-d_0 c_\mu] \quad (21)$$

Here $d_1 \geq 0$ requires that the solution for d_0 obey $2d_0 c_\mu \leq 1$.

If both μ_{opt} and τ_{opt} are measured, then the diffusion coefficient d_0 can be found from equating the two expressions for d_1 which results in a quadratic equation for d_0 with the roots

$$d_0 = \frac{1}{12c_\mu c_\tau} \left[2c_\mu + 3c_\tau \pm \sqrt{\frac{(2c_\mu - 3c_\tau)(2c_\mu^2 + 67c_\mu c_\tau + 3c_\tau^2)}{c_\mu - c_\tau}} \right]. \quad (22)$$

Once d_0 is determined, d_1 can be determined from either of Equations (18) or (20). Positivity of d_1 requires that the above solution obey $d_0 \leq 1/(2c_\mu)$ and $d_0 \leq 1/(3c_\tau)$. This solution for both diffusion coefficients d_0, d_1 is obtained without necessarily using the value of echo amplitude except for recording where it has a maximum. It uses the optimum tune shift and the optimum delay and could be useful when the BPM resolution is low. However this would require that all other beam conditions such as the dipole kick, quadrupole kick, bunch charge etc are kept exactly the same during both tune shift and delay scans. If this is not met, the solution given by Eq. (22) cannot be used.

For the (d_0, d_2) or (d_1, d_2) models discussed here, the optimum values of the tune shift and delay parameters must be found numerically.

B. Echo pulse width

In addition to the amplitude, the echo can also be characterized by the echo pulse width, e.g the full width at half maximum (FWHM) can be chosen as a width measure.

For the model $D(J) = D_0 + D_1(J/J_0)$, the FWHM can be found analytically from Eq. (11). We define a variable D_{up} which depends on an upper limit to the pulse full width $(\Delta t)_{FW}^{up}$ and other parameters as follows

$$D_{up} = \left(\frac{\varepsilon}{\mu \omega_{rev} \tau} \right)^2 \frac{2}{(\Delta t)_{FW}^{up}} \quad (23)$$

For example, with an upper limit to the pulse width of a 100 turns, we have $D_{up} = 2.6 \times 10^{-12} \text{m}^2/\text{s}$. For pulse widths $\Delta t_{FWHM} < (\Delta t)_{FW}^{up}$ such that $(D_0/D_{up}, D_1/D_{up}) \ll 1$, we can keep terms to first order in $D_0/D_{up}, D_1/D_{up}$, and we find for the FWHM

$$\Delta t_{FWHM} = 2\sqrt{2^{2/3} - 1} \left(\frac{\alpha}{\omega_{rev}\mu} \right) + 3 \left(\frac{\alpha\tau}{\omega_{rev}} \right)^2 \left[\frac{2^{2/3}}{3} d_0 + \frac{d_1}{\alpha} \right], \quad \alpha = 1 + \frac{1}{2} d_1 \mu^2 t_1^3 \quad (24)$$

As we see later, we have typically $(D_0/D_{up}, D_1/D_{up}) \approx 0.1$, so the above assumption is satisfied for pulse widths up to a 100 turns or somewhat larger. We find that the FWHM increases with increasing D_1 but very slowly with D_0 as seen in Fig. 2. When there is no diffusion, we have for the minimum FWHM

$$\Delta t_{FWHM}^{min} = \frac{2\sqrt{2^{2/3} - 1}}{\omega_{rev}\mu} \quad (25)$$

In units of turns, this theoretical minimum FWHM depends only on the tune shift coefficient μ . This value when compared with measured FWHM values can set limits on the tune shift parameter, as will be seen later.

For the other models with either (D_0, D_2) or (D_1, D_2) , the time dependent pulse shape and hence the FWHM must be found numerically. From this pulse shape, the upper envelope is found numerically as an interpolating function and the FWHM then calculated from this envelope function. Fig. 2 shows the dependence of the FWHM on the coefficients D_0, D_1, D_2 scaled by a parameter $D_{scale} = 2.4 \times 10^{-15} \text{m}^2/\text{s}$. The FWHM increases linearly with both D_0 and D_1 but with D_0 increases by only 3% over this range. The FWHM with D_2 increases the fastest and covers the range of values obtained from the RHIC data.

III. ANALYSIS OF RHIC DATA WITH AU IONS

We briefly discuss the experimental procedure here, more details can be found in [12]. The echo experiments were first done with Au ions, later with Cu ions and also with protons, all at injection energy. A special purpose quadrupole kicker was used with a rise time of $12.8\mu\text{s}$, about one revolution time in RHIC. The nonlinear tune shift was provided by a set of octupoles which are normally set to zero at injection, in order to observe the echoes. The initial dipole kick was delivered only in the horizontal plane by injection under a varying angle. Echoes were generated with different conditions including variable dipole and

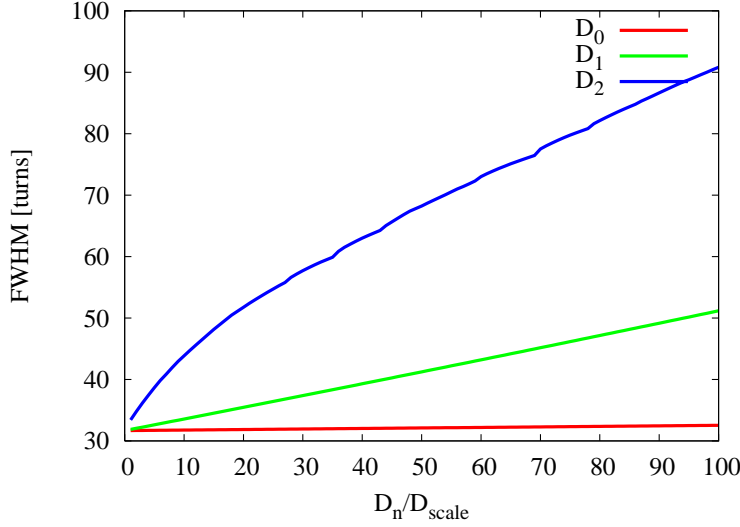


FIG. 2. FWHM as a function of the diffusion coefficients D_0, D_1, D_2 scaled by the value D_{scale} . Each curve shows the impact of the single coefficient with the others set to zero. The FWHM is calculated analytically from Eq. (24) for D_0, D_1 and numerically for D_2 . Parameters were taken from Table I, except for $\mu = 0.0077$.

Parameter	Nominal Value
Beam relativistic γ	10.52
Revolution time T_{rev}	12.8 μ s
Initial emittance ϵ_0 , un-normalized	1.6×10^{-7} m
Delay τ	450 turns
Initial tune shift parameter μ_0	0.0014
Quadrupole strength q	0.025
Quadrupole rise time	12.8 μ s

TABLE I. Relevant RHIC parameters for the echo experiments with Au ions.

quadrupole kicks, beam intensities, tunes, different delays between the dipole kick and the quadrupole kick and different octupole strengths. The emittance delivered to RHIC for each species was nearly constant. While echoes were observed with each species, the most consistent echoes were obtained with the Au ions and we will consider only those results in this article. Table I shows some of the relevant parameters for the Au ions [12].

A. Emittance growth and rescaling tune shift

In evaluating the tune shift parameter μ for calculating echo amplitudes, it is important to use the emittance following the dipole kick. The rms emittance is given by

$$\begin{aligned}\varepsilon &= \frac{1}{\beta} [\langle x^2 \rangle \langle p^2 \rangle - (\langle xp \rangle)^2]^{1/2} \\ &= 2[\langle J \cos^2 \phi \rangle \langle J \sin^2 \phi \rangle - \langle J \sin \phi \cos \phi \rangle^2]^{1/2}\end{aligned}\quad (26)$$

The ensemble averages are calculated using the distribution function at time t after the dipole kick which can be written in the notation of [15] as

$$\psi_2(J, \phi, t) = \psi_0(J + \theta \sqrt{2\beta J} \sin(\phi - \omega(J)t) + \frac{1}{2}\beta_K \theta^2) \quad (27)$$

and the averages are found from e.g. $\langle J \cos^2 \phi \rangle = \int dJ d\phi J \cos^2 \phi \psi_2(J, \phi, t)$ etc. It can be shown this leads to an rms emittance given by

$$\begin{aligned}\varepsilon(t) &= [(J_0 + \frac{1}{2}\beta_K \theta^2)^2 - A_2(t)^2]^{1/2} \\ A_2(t) &= \frac{\beta_K \theta^2}{2(1 + \Theta_2^2)^{3/2}} \exp[-\frac{\beta_K \theta^2}{2J_0} \frac{\Theta_2^2}{1 + \Theta_2^2}], \quad \Theta_2 = 2\omega' J_0 t\end{aligned}\quad (28)$$

At times $t \gg \tau_D$, the term $A_2 \rightarrow 0$ and we can approximate

$$\varepsilon = J_0 + \frac{1}{2}\beta_K \theta^2 = \varepsilon_0 [1 + \frac{1}{2}(\frac{\Delta x}{\sigma_0})^2] \quad (29)$$

where $\varepsilon_0 = J_0$ is the initial emittance, $\Delta x = \sqrt{\beta_K \beta} \theta$ is the change in beam position at the BPM and $\sigma_0 = \sqrt{\beta \varepsilon_0}$ is the initial beam size at the BPM. The last expression in Eq. (29) has the same form as in [18]. Thus a kick to a 3σ amplitude results in an emittance which is 5.5 times larger than the initial emittance. We will take this as an average estimate for the emittance following the dipole kick. By definition, the tune shift parameter μ increases linearly with emittance and hence μ increases from its nominal value of 0.0014 to 0.0077 following the dipole kick. Without this rescaling, the model cannot agree with the experimental results, as seen in the earlier analysis [12, 13].

B. Diffusion coefficients from optimum tune shift and delay

The theory predicts that the maximum echo amplitude, which occurs close to the time 2τ after the dipole kick, grows indefinitely with the product $\mu\tau$ in the absence of diffusion. In the presence of any diffusion, the echo amplitude grows more slowly, reaches a maximum and then decreases as either μ or τ is increased. In each case, the irreversible particle motion caused by the presence of diffusion reduces the amplitude of the recohering signal at the time of the echo. Here we will apply the formulas developed in Section II A to extract diffusion coefficients from measurements of the optimal tune shift and optimal delay.

We discuss first the analysis of the nonlinear tune shift scan done on March 11, 2004. During this scan, the quadrupole kick and delay between the dipole kick and quadrupole kick were kept constant. Octupole strengths were set to values $K_3 = (1.5, 2, 2.5, 5, 6, 7, 8, 9, 10) \text{ m}^{-3}$. The nominal value was $K_3 = 7 \text{ m}^{-3}$ corresponding to a nominal tune shift parameter $\mu_0 = 0.0014$ before the dipole kick. Echoes were observed for all $K_3 \geq 2.5 \text{ m}^{-3}$. The largest echoes were observed at $K_3 = 5 \text{ m}^{-3}$ which corresponds to a nominal tune shift parameter $\mu = 0.001$ while the rescaled tune shift value is $\mu_{opt} = 0.0055$.

For the D_0, D_1 model, the starting solutions were obtained by solving Eqs. (20) and (21). These yielded $d_0 = 2.245 \times 10^{10} \text{ s}^{-3}$, $d_1 = 2.435 \times 10^{10} \text{ s}^{-3}$, which lead to $D_0 = 1.08 \times 10^{-13} \text{ m}^2/\text{s}$ and $D_1 = 1.17 \times 10^{-13} \text{ m}^2/\text{s}$. These found values for (D_0, D_1) yield a maximum at $\mu_{opt} = 0.0055$ by design but the amplitude values decrease more slowly with μ than the data. To improve the fit with the data, a numerical fitting was done (using Mathematica [19]) to the data with the model shown in Eq. (11). These yielded $D_0 = 1.62 \times 10^{-13} \text{ m}^2/\text{s}$ and $D_1 = 1.19 \times 10^{-13} \text{ m}^2/\text{s}$ and led to a better fit with all the data. These values for D_0, D_1 were labeled as $D_{0,sc}, D_{1,sc}$ respectively and subsequent values were scaled by these values for convenience. With both the (D_0, D_2) and the (D_1, D_2) models, a least square minimization was done to fit the data against the respective models for the amplitude. The fit for D_2 from the (D_0, D_2) model was similarly labeled as $D_{2,sc}$. The resulting fits and the data are shown in Fig.3. The values of the coefficients are shown in Table II. Relative to the previous comparison of theory with experimental data cf. Fig. 4 in [12], these fits show significant improvement. Of the three models, the best fit with the lowest chi squared is seen with the (D_0, D_2) model with the next best being the (D_1, D_2) model. However the

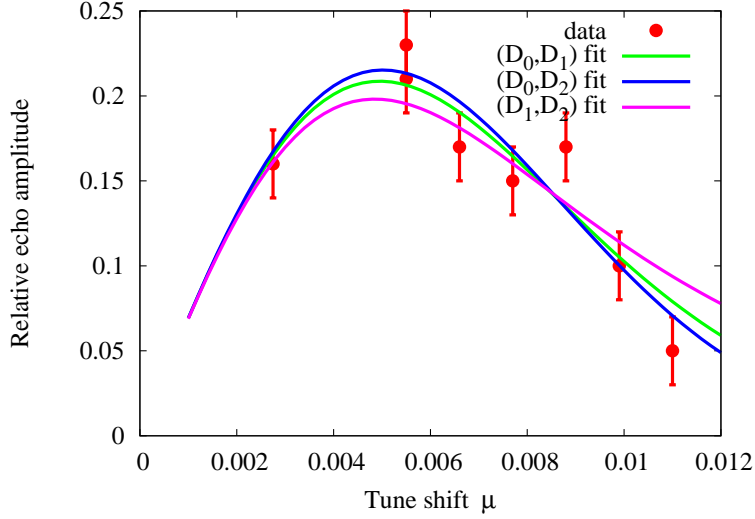


FIG. 3. Comparison of the echo amplitude vs tune shift strength scan. The data shown in red with error bars while the fits shown are with the three models for the diffusion coefficients discussed in the text.

models are fairly close and no model can be ruled out based on this data.

On a later day (March 17, 2004), the delay τ between the dipole kick and the quadrupole kick was varied with values (450, 500, 550, 600, 900) turns. Echoes were only observed at the first three values of the delay. In all six echoes were observed with the largest amplitudes at 450 turns. The quadrupole kick strength, the octupole strengths and the tunes were kept constant. We will use this limited data set to obtain the diffusion coefficients from the delay scan.

For the (D_0, D_1) model, we start by solving Eq. (18) and Eq. (19) for the coefficients from the echo amplitude and the value of the optimum delay τ_{opt} . Again, better fits to the data are obtained by a least square minimization which is also the procedure for the other two models. Table II shows the best fit values with this delay scan. Compared to the values from the tune shift scan, the coefficients for the same model are within a factor of two from this delay scan. Some of the variation in the values between the scans can be due to different beam conditions on the two days such as bunch intensities and machine tunes. However the uncertainties associated with these values are large since there were too few data points. Fig. 4 shows the comparison of the fitted models with the data. Again all three

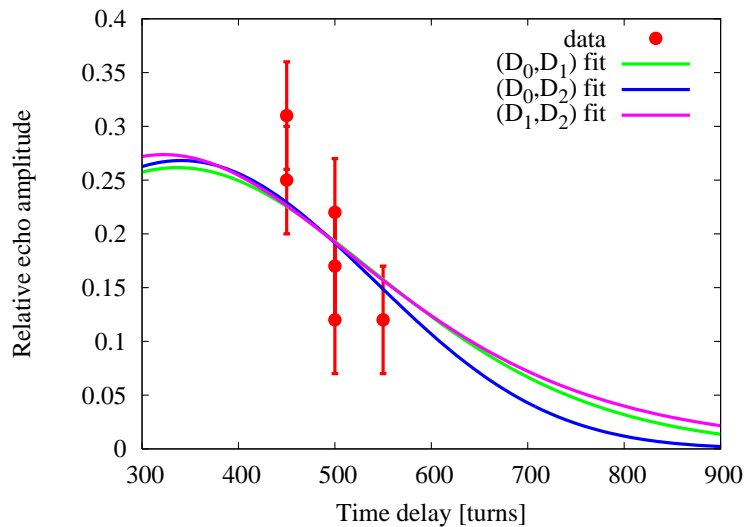


FIG. 4. Comparison of the echo amplitude vs time delay between the dipole and quadrupole kicks. The data shown with error bars while the fits are shown with the three models discussed in the text.

Model	Tune Shift scan	Delay scan
D_0 / D_1	1.6 / 1.3	0.65 / 1.3
D_0 / D_2	1.9 / 0.025	3.7 / 0.015
D_1 / D_2	2.3 / 0.025	1.9 / 0.013

TABLE II. Comparison of the diffusion coefficients from the tune shift and delay scans. All diffusion coefficients are in units of $10^{-13} \text{ m}^2/\text{s}$.

models show similar goodness of fits with the best fit (minimum chi squared) obtained with the (D_0, D_2) model but all chi squared values are close. All models show that the relative echo amplitude reaches a maximum at around 390 turns which is less than the minimum delay of 450 turns used in the experiment.

C. Diffusion coefficients from the echo amplitude and the FWHM

The above analysis has shown that all three models are viable candidates in describing the data dependence on either the tune shift or the delay. We now use turn by turn (TBT) data to fit both the echo amplitude and the echo pulse width with each model. Ten such data

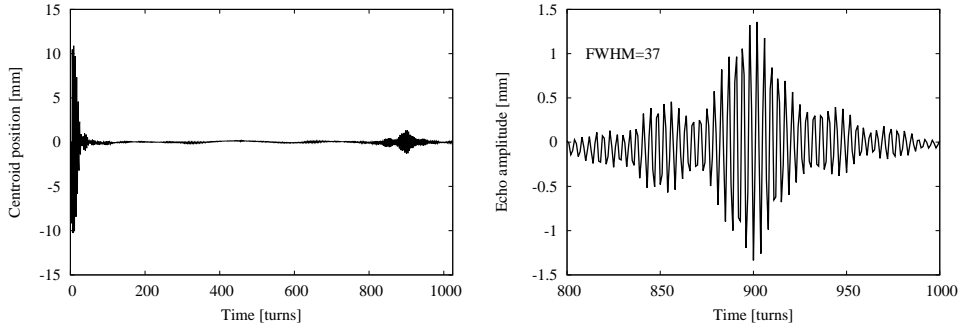


FIG. 5. The entire centroid position turn by turn (left) and the echo pulse isolated (right) for the data with the shortest FWHM. Here the centroid decoheres cleanly after the dipole kick. The quadrupole kick was applied at turn 450.

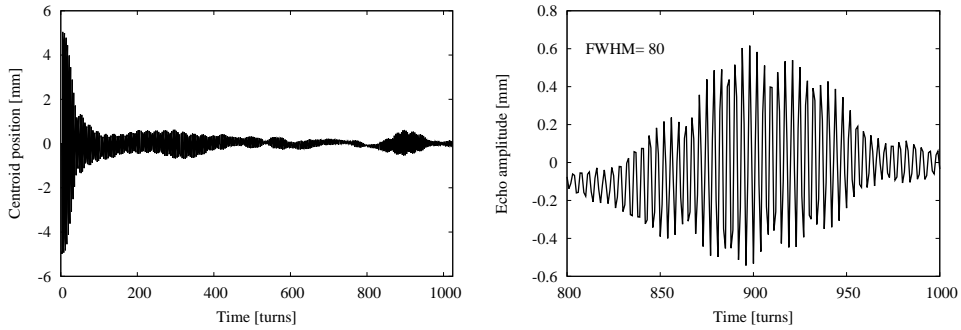


FIG. 6. The entire centroid position turn by turn (left) and the echo pulse isolated (right) for the data with the largest FWHM. Notice the much larger and longer ringing of the centroid after the dipole kick. The quadrupole kick was applied again at turn 450.

sets could be retrieved from the 2004 measurements. In this TBT set, the initial dipole kick and bunch charge varied but the other parameters including the quadrupole kick strength, tunes, delay and octupole strengths were kept constant. Figures 5 and 6 show two examples from this set, one with a clean echo pulse and the other where the beam centroid takes a longer time to decohere after the initial kick and the echo pulse is also much wider. Some of the more distorted signals could be due to oscillations from off-axis injection and could partly be due to a fourth order resonance and slightly higher bunch charge. For each data set, an interpolating function was found to fit the upper envelope of the echo pulse and the FWHM was extracted from this interpolating function. Using the value of the rescaled tune shift parameter $\mu = 0.077$, the minimum theoretical value of the FWHM without

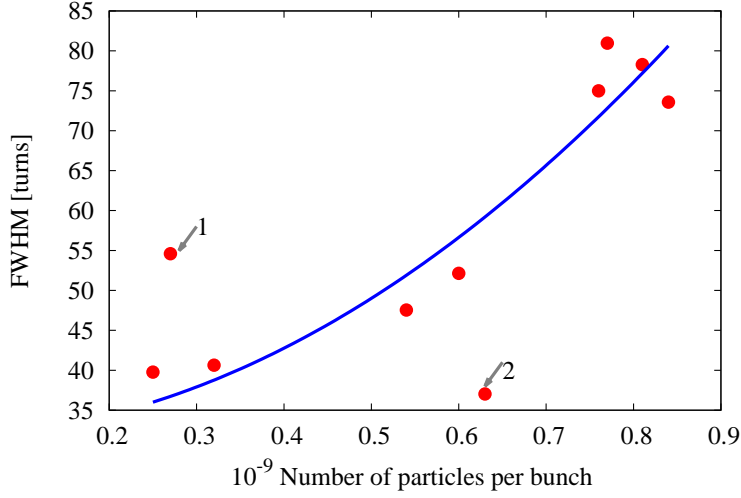


FIG. 7. FWHM vs the number of particles per bunch. Except for the points labeled 1 and 2, all the other data points show an increasing FWHM with bunch charge. The blue curve shows a quadratic fit through these points.

diffusion, using Eq. (25), is 32 turns. This is consistent with the minimum FWHM with diffusion from the data set which is 37 turns. The bare tune shift parameter of $\mu_0 = 0.0014$ would have predicted a minimum FWHM of 160 turns, much larger than any FWHM value measured.

Fig. 7 shows the FWHM plotted as a function of the number of particles per bunch. This figure shows that the FWHM fell into three distinct clusters because the bunch charge varied around three values. Except for the two outlier points labeled as (1, 2), all other points show that the FWHM increases with charge. These other points are fit to a power law curve

$$FWHM(N) = \Delta t_{FWHM}^{min} + aN^p \quad (30)$$

where Δt_{FWHM}^{min} is the minimum FWHM from Eq. (25), N is the number of particles per bunch and (a, p) are the fit parameters. The fit shows that the exponent is $p = 2.002$, so the FWHM increases quadratically with the charge. Since the tune shift, delay, and tune were kept constant during these measurements, the outlier points show that the FWHM values may depend on other parameters, such as the initial dipole kick amplitude.

We now solve for two diffusion coefficients using the relative echo amplitude and the

FWHM. For the (D_0, D_1) model, the FWHM can be found analytically, as shown in Eq. (24). The d_0 coefficient can be written as a function of the echo amplitude and d_1 using the echo amplitude equation Eq.(11) as

$$d_0 = -\frac{1}{\mu^2 \tau^3} \ln \left[\frac{\langle x \rangle_{rel}^{amp}}{2\pi q \mu N_{delay}} (1 + \mu^2 \tau^3 d_1)^{3/2} \right] \quad (31)$$

where $\langle x \rangle_{rel}^{amp} = \langle x \rangle^{amp} / (\beta_K \theta)$ is the relative echo amplitude in terms of the dipole kick and $N_{delay} = \tau / T_{rev}$ is the delay in units of turns. The positivity of d_0 implies an upper limit to d_1 as

$$d_1^{max} = \frac{1}{\mu^2 \tau^3} \left[\left(\frac{2\pi q \mu N_{delay}}{\langle x \rangle_{rel}^{amp}} \right)^{1/3} - 1 \right] \quad (32)$$

The value of d_1 can be found by numerically solving the equation Eq. (24) for the FWHM with d_0 substituted from Eq. (31). We find that this (D_0, D_1) model yields positive d_0 coefficients in only four of the ten cases. We conclude therefore that the D_0, D_1 model is not well suited for this data.

With the (D_0, D_2) model, the d_0 coefficient can again be found analytically as a function of the echo amplitude and d_1 using

$$d_0 = -\frac{1}{\mu^2 \tau^3} \ln \left[\frac{\langle x \rangle_{rel}^{amp}}{\pi q \mu N_{delay}} \frac{1}{\text{Im}[e^{i\Phi_0(T_{rev})} H_{02}(T_{rev})]} \right] \quad (33)$$

where H_{02} is defined in Eq. (13). We find again that no solutions with positive D_0 can be found in all cases with FWHM > 70 turns. Even in other cases where the solutions can be found, the values of D_2 are significantly larger than the values found in the previous sections, hence appear to be in a disconnected region of the parameter space. Since D_0 has little impact on the FWHM (see Fig. 2), in both the (D_0, D_1) and (D_0, D_2) models, large values of the FWHM can make D_1 or D_2 large which then require a negative D_0 to satisfy the amplitude condition. Thus fitting the models to both the amplitude and FWHM rules out the models with D_0 .

In the case of the D_1, D_2 model, neither coefficient can be found analytically from the amplitude equation. Instead the amplitude and the FWHM equations must be solved numerically. Figure 8 shows the forms of the function $\text{ampl}(d_1, d_2)$ and $\text{fwhm}(d_1, d_2)$. Also shown are the intersections of these surfaces with the plane of constant amplitude or FWHM value respectively. In each case, the intersection of the surface with the plane

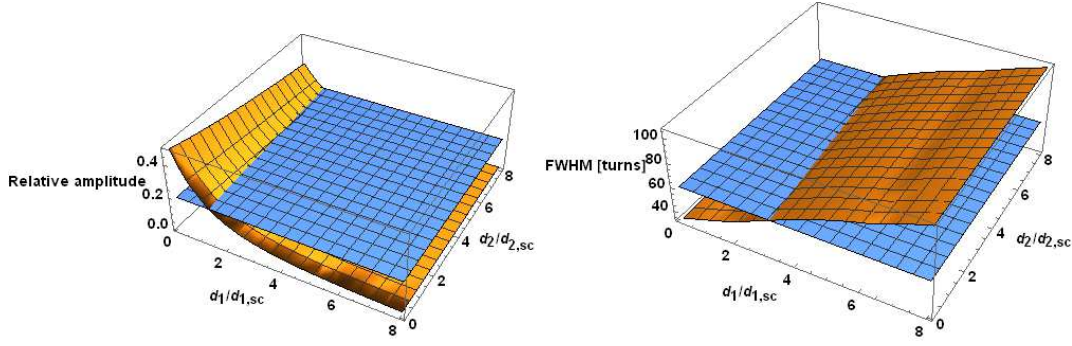


FIG. 8. Left: Relative echo amplitude (in brown) as a function of the scaled diffusion coefficients $d_1/d_{1,sc}, d_2/d_{2,sc}$ intersected by a plane (in blue) of a particular relative amplitude value, here chosen to be 0.2. The intersection defines the family of solutions for (d_1, d_2) at this amplitude. Right: The FWHM (in brown) as a function of the same scaled variables and the plane (in blue) at a constant FWHM, here chosen to be 60 turns. Again, the intersection defines the family of solutions for the FWHM equation.

determines a curve of solutions for that equation. The intersection of the two curves in the d_1, d_2 plane would determine the required solution for given values of the amplitude and FWHM. In this figure the values of d_1, d_2 are scaled by $d_{1,sc}, d_{2,sc}$ which are obtained from $D_{1,sc}, D_{2,sc}$ using Eq. (9). These plots demonstrate that for the range of measured values of the echo amplitude and the FWHM, solutions for the diffusion coefficients exist in the range $0 \leq (d_1/d_{1,sc}, d_2/d_{2,sc}) \leq 8$.

It turns out to be easier to do a least squared minimization to find the solution. Here we define the χ^2 function as

$$\chi^2 = \left(\frac{\text{ampl}(d_1, d_2) - \text{ampl}_{\text{data}}}{\sigma_{\text{ampl}}} \right)^2 + \left(\frac{\text{fwhm}(d_1, d_2) - \text{fwhm}_{\text{data}}}{\sigma_{\text{fwhm}}} \right)^2 \quad (34)$$

where $\text{ampl}(d_1, d_2)$ and $\text{fwhm}(d_1, d_2)$ are the amplitude function (from Eq. (16)) and the FWHM function defined numerically and $\sigma_{\text{ampl}} = 0.05$ and $\sigma_{\text{fwhm}} = 2$ are the estimated uncertainties in the two data variables. This least squares method turns out to be efficient and leads to positive solutions for d_1, d_2 in all cases. Table III shows the values of the diffusion coefficients in these cases. We observe that these values are close to the values of D_1 found from the optimal tune shift and delay measurements shown in Table II. The D_2 values differ by an order of magnitude in the two tables but considering that the delay and

Particles per bunch [10^9]	Rel. ampl. []	FWHM [turns]	D_1 [10^{-13} m ² /s]	D_2 [10^{-13} m ² /s]
0.25	0.245	39.8	1.28	0.0030
0.27	0.225	54.6	0.13	0.51
0.32	0.160	40.6	1.49	0.32
0.54	0.127	47.5	2.00	0.28
0.6	0.142	52.1	1.98	0.21
0.63	0.125	37.0	1.98	0.30
0.76	0.114	75.0	2.53	0.24
0.77	0.122	81.0	2.18	0.24
0.81	0.110	78.3	2.53	0.24
0.84	0.0998	73.6	2.53	0.24

TABLE III. Diffusion coefficients (D_1, D_2) found using the amplitude and the FWHM values from the turn by turn data.

tune shift scan methods for the amplitude are less sensitive to D_2 and also from the larger number of data points in the FWHM analysis, we expect the values in Table III to be more accurate. In most cases, the D_1 coefficient is an order of magnitude greater than D_2 . The single exception (row 2 of this table) corresponds to the outlier point labeled 1 in Fig. 7. As a function of charge, D_1 increases while D_2 appears to be independent of the charge.

D. Diffusion dependence on bunch charge

We focus now on the (D_1, D_2) model which is the only one of those studied that can describe both the amplitude and pulse width of the echo. During the measurements on March 17, 2004 an intensity scan was done with all other parameters kept constant. While the turn by turn data from that scan is not easily accessible, the echo amplitudes are available with 27 data points. This data can be used to measure the diffusion coefficients as a function of bunch charge.

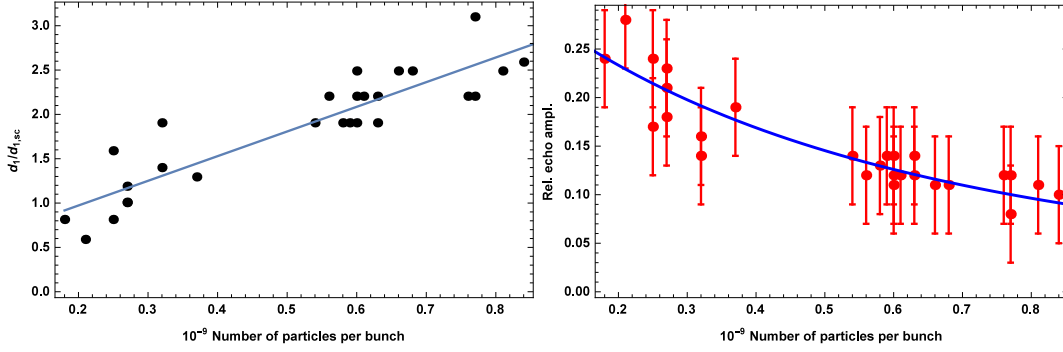


FIG. 9. Left: Calculated d_1 values as a function of the number of particles per bunch and the linear fit to the values. Right: Measured relative echo amplitude (red) at different intensities and compared with the best fit curve (blue) with (D_1, D_2) , with D_1 from the linear fit in the left plot and D_2 independent of the bunch charge.

Both (D_1, D_2) coefficients can be found by a least square minimization of the fit to the amplitude. This process allows a determination of (D_1, D_2) as a function of charge, The left plot in Fig. 9 shows the D_1 values found and a linear fit to the values. This confirms the behavior seen in the previous section but now with a larger data set. Similarly as earlier, the D_2 values are nearly independent of the charge. We can parameterize the echo amplitude's dependence on bunch charge via these fits for D_1, D_2 and the amplitude equation (16). The linear fit yields $d_1/d_{1,sc} = 0.42 + 2.78N$ where N is the number of particles per bunch in units of 10^9 while for d_2 we take the mean value over this set, $d_2/d_{2,sc} = 6.24$ The right plot in Fig. 9 shows the measured echo amplitudes (in red) as a function of the number of particles per bunch and also the calculated amplitude (in blue) from these fits for (D_1, D_2) . The measured echo amplitude decreases with increasing charge, and this trend is well reproduced by the theoretical amplitude function. This is a consistency check and is to be expected, since the linear fit for d_1 and constant for d_2 were obtained from the data set. The comparison in Fig. 9 shows that we can parameterize the diffusion coefficients as

$$D(J) = [a_{10} + a_{11}N] \left(\frac{J}{J_0}\right) + a_{20} \left(\frac{J}{J_0}\right)^2 \quad (35)$$

where a_{10}, a_{11}, a_{20} are functions of machine and beam parameters such as the nonlinearity, tunes, emittance etc. but independent of the bunch charge.

Space charge effects and intra-beam scattering (IBS) are the dominant source of particle

diffusion for heavy ions such as Au in RHIC, at injection energy. The incoherent space charge and IBS induced diffusion and emittance growth depends linearly on the charge and our analysis confirms that the leading diffusion coefficient D_1 increases linearly with charge. The coefficient D_2 is likely to be determined by diffusion from single particle nonlinear dynamics processes.

In the above analysis we have neglected the effect of wakefields on the echo formation. Their impact on the calculations above is not likely to be significant. As seen in Figures 5 and 6 and generally true for the available turn by turn data, the centroid response after the dipole kick is cleaner and the relative echo amplitude is larger with the larger amplitude kick. This would likely not be the case if the effects of the transverse wake were significant. Instead, effects due to injection oscillations and fourth order resonance which shows up at intermediate amplitudes are the likely reason for the response seen in Fig. 6. In addition, the effect of wake fields would be visible in a change in the decoherence time with intensity. An analysis of the intensity scan data shows no correlation between the decoherence time and the bunch intensity.

IV. MEAN ESCAPE TIME

One useful time scale that can be extracted from the diffusion coefficients is the mean escape time t_{esc} associated with probabilistic processes [20]. This time, also known as the mean first passage time, is the mean time taken (averaging over many realizations of the process) for a particle to escape from a certain region defined by a boundary. It was shown in [21] that in the case that $D(J) = D_1(J/J_0)$, the time dependent density distribution solution $\psi(J, t)$ to the diffusion equation leads to a beam lifetime t_L which is close to the escape time t_{esc} estimate. Defining $t_L = -N(t)/(dN/dt)$ where $N(t) = \int \psi(J, t) dJ$ is the particle number, it was shown that

$$t_L \approx 0.7 \frac{J_A J_0}{D_1}, \quad t_{esc} = \frac{J_A J_0}{D_1} \quad (36)$$

where J_A is the action at the absorbing boundary. We will assume that the mean escape time is also a useful beam relevant time scale when $D(J) = D_1(J/J_0) + D_2(J/J_0)^2$.

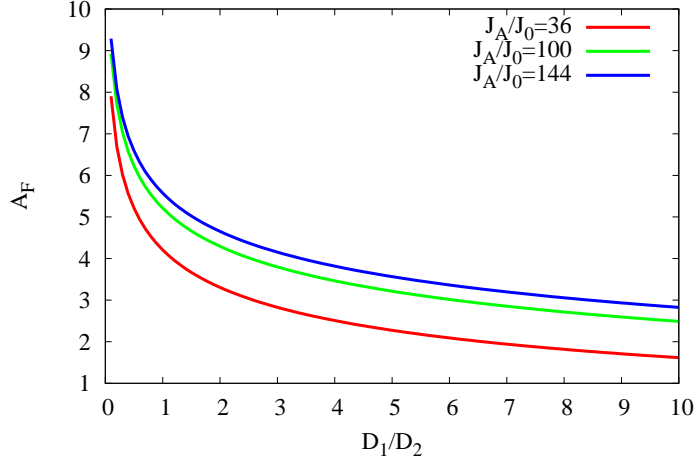


FIG. 10. Dependence of A_F , defined in Eq. (38), on the ratio of diffusion coefficients D_1/D_2 for three values of the ratio of the action at the absorbing aperture J_A to the initial emittance J_0 .

The mean escape time from an action J to an absorbing boundary at action J_A is given by

$$\begin{aligned}
 t_{esc}(J) &= \int_J^{J_A} dJ \frac{J}{D(J)} = \int_J^{J_A} dJ \frac{J}{D_1(J/J_0) + D_2(J/J_0)^2} \\
 &= \frac{J_0^2}{D_2} \ln \left[\frac{D_1 + D_2(J_A/J_0)}{D_1 + D_2(J/J_0)} \right]
 \end{aligned} \tag{37}$$

This is the mean escape time for particles initially at a single action J to reach the aperture at action J_A due to diffusion. A parameter describing the escape time for the beam can be obtained by averaging this over the initial beam distribution $\psi_0(J)$, which yields

$$\begin{aligned}
 \langle t_{esc} \rangle &= \frac{J_0}{D_2} \int_0^\infty dJ \exp\left[-\frac{J}{J_0}\right] \ln \left[\frac{D_1 + D_2(J_A/J_0)}{D_1 + D_2(J/J_0)} \right] \\
 &= \frac{J_0^2}{D_2} \left[\ln \left(\frac{D_1}{D_2} + \frac{J_A}{J_0} \right) - \ln \frac{D_1}{D_2} - e^{D_1/D_2} \Gamma \left(0, \frac{D_1}{D_2} \right) \right] \equiv \frac{J_0^2}{D_2} A_F
 \end{aligned} \tag{38}$$

where $\Gamma(0, z)$ is the incomplete Gamma function and we have assumed $D_2 \neq 0$. The dimensionless amplifying factor A_F , defined by the terms in square brackets, depends only the ratios $D_1/D_2, J_A/J_0$, Figure 10 shows the dependence of the dimensionless terms on D_1/D_2 for three values of J_A/J_0 corresponding to apertures at $(6, 10, 12)\sigma$ respectively. For $D_1/D_2 \simeq 10$, A_F is of order unity. Hence the mean escape time is determined primarily by J_0^2/D_2 . In the case that $D_2 = 0$, the time scale would be determined by $J_0 J_A/D_1$. With

$J_0 = 1.6 \times 10^{-7} \text{m}$, and taking a representative value $D_2 = 0.25 \times 10^{-13} \text{ m}^2/\text{s}$ from Table III, we have $\langle t_{esc} \rangle \approx 1 \text{s}$. While this time is extremely short, it corresponds to the lifetime of a beam at large amplitudes and not to a beam circulating on the nominal closed orbit. Observations in RHIC did show that lifetimes of kicked beams were significantly smaller compared to that for beams not kicked. However the early losses of the kicked beams were dominated by scraping at aperture restrictions, so there is no straightforward way to determine the contribution of diffusion to those lifetimes. Nevertheless, the diffusion coefficients and the associated time scales should be useful for relative measures of beam growth and particle loss. As an example, it could be useful in IOTA to quickly distinguish between lattices with different degrees of integrability. If echoes can be generated by small amplitude kicks, then the calculated diffusion coefficients and the time scales would be more representative of beam behavior under nominal conditions. Determining the diffusion coefficients may require different parameterizations of $D(J)$ at small and large amplitudes, as seen for example in [16].

V. SUMMARY

In this article, we revisited earlier observations of transverse beam echoes in RHIC to extract diffusion coefficients from those measurements. We considered three models for the action dependence of the diffusion coefficients: $D(J) = D_0 + D_1(J/J_0)$, $D(J) = D_0 + D_2(J/J_0)^2$, and $D(J) = D_1(J/J_0) + D_2(J/J_0)^2$. All three models were found to adequately describe the echo amplitudes measured during scans of the nonlinear tune shift and the delay between the dipole and quadrupole kicks. Next, turn by turn data was used to extract both the amplitude and the FWHM of the pulse width. Here both models with D_0 do not describe the data with larger pulse widths, so the only model that successfully describes both the amplitude and the FWHM data is the (D_1, D_2) model. We find that D_1 is an order of magnitude larger than D_2 in most cases; it increases linearly with the charge while D_2 is nearly independent of the charge. Using these charge dependencies, the (D_1, D_2) model also adequately describes another set of data where the echo amplitudes were measured as a function of charge.

These results show that transverse echoes can indeed be used to measure transverse

beam diffusion in existing and future hadron synchrotrons, We make some observations on requirements for future measurements. The diffusion measurements require good control of several machine and beam parameters such as the initial dipole kick, the quadrupole kick, machine nonlinearity, tunes and beam emittance, to name the most important. Injection oscillations can strongly influence the echo amplitude and pulse shape, so these need to be controlled to the extent possible. Alternatively if available, a fast dipole kicker in the ring would be preferable to initiate the echo. In such a case, a transverse damper can damp initial oscillations and then be turned off before the dipole kicker is used. While the echo amplitude variation with scans of the tune shift and time delay are useful, detailed analysis of the turn by turn data yields more information. As an example of this, we found that the FWHM scales quadratically with the charge and therefore is more sensitive to intensity changes than the echo amplitude. The proximity of resonances can also spoil echoes so the tunes and the dipole kick amplitudes need to be chosen carefully as well.

Acknowledgments

Fermilab is operated by Fermi Research Alliance, LLC under U.S. Department of Energy contract No. DE-AC02-07CH11359. BNL is operated by Brookhaven Science Associates, LLC under U.S. Department of Energy contract No. DE-AC02-98CH10886.

-
- [1] K. Mess and M. Seidel, Nucl. Instr. & Meth. A **351**, 279 (1994)
 - [2] W. Fischer, M. Giovannozzi and F. Schmidt, Phys. Rev. E, **55**, 3507 (1997).
 - [3] R.P. Fliller III, A. Drees, D. Gassner, G. McIntyre, S. Peggs, D. Trbojevic,, Proceedings of PAC 2003, 2904 (2003).
 - [4] G. Valentino, R. Assmann, R. Bruce, F. Burkart, V. Previtali, S. Redaelli, B. Salvachua, G. Stancari, A. Valishev, PRST-AB, **16**, 021003 (2013)
 - [5] G. Stancari, Proceedings of HB2014, 294 (2014).
 - [6] G.V. Stupakov, Preprint, SSCL-579 (1992)
 - [7] G.V. Stupakov and S.K. Kaufmann, Preprint SSCL-587 (1992)
 - [8] G.V. Stupakov and A.W. Chao, Proceedings of PAC97, 1834 (1997)

- [9] L.K. Spentzouris, J-F. Ostiguy, P.L. Colestock, *Phys. Rev. Lett.*, **76**, 620 (1996)
- [10] O. Bruning, T. Linnekar, F. Ruggiero, W. Scandale, E. Shaposhnikova, D. Stellfeld, *Proceedings of PAC97*, 1816 (1997)
- [11] G. Arduini, F. Ruggiero, F. Zimmermann, M. Zorzano-Mier, Preprint CERN-SL-Note-2000-048-MD (2000)
- [12] W. Fischer, T. Satogta and R. Tomas, *Proceedings of PAC2005*, 1955 (2005)
- [13] S. Sorge, O. Boine-Frankenheim, and W. Fischer, *Proceedings of ICAP 06*, 234 (2006).
- [14] S. Nagaitsev, A. Valishev, V.V. Danilov, D.N. Shatilov, *Proceedings of IPAC12*, 16 (2012)
- [15] A.W. Chao, Lecture Notes at www.slac.stanford.edu/~achao/lecturenotes.html
- [16] T. Chen et al, *Phys. Rev. Lett.*, **68**, 33 (1992)
- [17] F. Zimmermann, *Part. Acc.*, **49**, 67 (1995)
- [18] D. Edwards and M.J. Syphers, *Introduction to the Physics of High Energy Accelerators*, Wiley, New York (1993)
- [19] Wolfram Research Inc., *Mathematica*, Version 10.4, Champaign, IL (2016)
- [20] C.W. Gardiner, *Handbook of Stochastic Methods*, Springer (1985)
- [21] T. Sen, *JINST*, **6**, 10017 (2011)